RESEARCH BRIEF

OTX2 Activity at Distal Regulatory Elements Shapes the Chromatin Landscape of Group 3 Medulloblastoma

Gaylor Boulay[1,2], Mary E. Awad[1], Nicolo Riggi[3], Tenley C. Archer[2,4], Sowmya Iyer[1], Wannaporn E. Boonseng[1], Nikki E. Rossetti[1], Beverly Naigles[1], Shruthi Rengarajan[1], Angela Volorio[1,3], James C. Kim[1], Jill P. Mesirov[2,5], Pablo Tamayo[2,5], Scott L. Pomeroy[2,4], Martin J. Aryee[1,2], and Miguel N. Rivera[1,2]

ABSTRACT

Medulloblastoma is the most frequent malignant pediatric brain tumor and is divided into at least four subgroups known as WNT, SHH, Group 3, and Group 4. Here, we characterized gene regulation mechanisms in the most aggressive subtype, Group 3 tumors, through genome-wide chromatin and expression profiling. Our results show that most active distal sites in these tumors are occupied by the transcription factor OTX2. Highly active OTX2-bound enhancers are often arranged as clusters of adjacent peaks and are also bound by the transcription factor NEUROD1. These sites are responsive to *OTX2* and *NEUROD1* knockdown and could also be generated *de novo* upon ectopic *OTX2* expression in primary cells, showing that OTX2 cooperates with NEUROD1 and plays a major role in maintaining and possibly establishing regulatory elements as a pioneer factor. Among OTX2 target genes, we identified the kinase NEK2, whose knockdown and pharmacologic inhibition decreased cell viability. Our studies thus show that OTX2 controls the regulatory landscape of Group 3 medulloblastoma through cooperative activity at enhancer elements and contributes to the expression of critical target genes.

SIGNIFICANCE: The gene regulation mechanisms that drive medulloblastoma are not well understood. Using chromatin profiling, we find that the transcription factor OTX2 acts as a pioneer factor and, in cooperation with NEUROD1, controls the Group 3 medulloblastoma active enhancer landscape. OTX2 itself or its target genes, including the mitotic kinase NEK2, represent attractive targets for future therapies. *Cancer Discov; 7(3); 288–301. ©2017 AACR.*

INTRODUCTION

Brain tumors are a leading cause of cancer-related death in children, and medulloblastoma is the most common malignant brain tumor type (1). Over the last decade, expression profiling of large cohorts of primary tumors led to the identification of at least four main molecular medulloblastoma variants (2–6), which differ in prognosis and demographic properties (7). DNA-sequencing studies, focusing on both point mutations and copy-number changes, have further reinforced these distinctions and show specific patterns of DNA alterations in each subtype (8–11). At a mechanistic

[1]Department of Pathology and Center for Cancer Research, Massachusetts General Hospital and Harvard Medical School, Boston, Massachusetts. [2]Broad Institute of Harvard and MIT, Cambridge, Massachusetts. [3]Institute of Pathology, Centre Hospitalier Universitaire Vaudois, Faculty of Biology and Medicine, University of Lausanne, Lausanne, Switzerland. [4]Department of Neurology, Boston Children's Hospital and Harvard Medical School, Boston, Massachusetts. [5]Department of Medicine, University of California, San Diego, La Jolla, California.

Note: Supplementary data for this article are available at Cancer Discovery Online (http://cancerdiscovery.aacrjournals.org/).

Corresponding Author: Miguel N. Rivera, Massachusetts General Hospital, 149 13th Street, Building 149, Charlestown, MA 02129. Phone: 617-643-7384; Fax: 617-726-5684; E-mail: mnrivera@mgh.harvard.edu

doi: 10.1158/2159-8290.CD-16-0844

level, the best understood subtypes are characterized by deregulation of either the WNT or the SHH pathway and are presumed to originate from specific precursor cell populations during development (12). The two remaining groups, known as Group 3 and Group 4, account for 60% of tumors but are poorly understood. Given the limited treatment options available for these tumors, further understanding of their biological basis could have major implications for therapy. This is particularly relevant for Group 3 tumors, which have the poorest outcomes.

Transcriptional regulation plays a central role in determining cell fate and identity in development and cancer. Master transcription factors have a major impact on transcriptional programs, as dramatically demonstrated by reprogramming experiments where differentiated cells are converted into pluripotent stem cells by the exogenous expression of a combination of transcription factors (13). Similar reprogramming strategies can also modify the tumor-propagating potential of tumor cells (14–17). These transcriptional programs are controlled by promoters and by highly lineage-specific distal regulatory elements (18, 19), also called enhancers, that define the regulatory landscape of a given cell type. Rapidly advancing knowledge of the "histone code" of post-translational modifications and the combined use of chromatin immunoprecipitation with next-generation sequencing have greatly facilitated the large-scale identification of regulatory elements and have shown their importance in normal cells and cancer (18, 20–22). In the case of medulloblastoma, a recent study has shown that different subgroups have distinct sets of super-enhancers (23).

In this study, we sought to gain insight into the mechanisms of gene regulation that drive Group 3 medulloblastoma. We find that the transcription factor OTX2, which has been implicated in cell proliferation and tumorigenicity in medulloblastoma (24–26), is present at most active enhancers in primary Group 3 tumors. In keeping with this finding, *OTX2* is highly expressed in all Group 3 tumors and is in fact amplified in 8% of cases, making it the second most amplified gene after *MYC* (27). *OTX2* is also expressed in the WNT and Group 4 subtypes, suggesting that it may play an important role in the majority of medulloblastomas. Although OTX2 binds a large number of active and inactive sites across the genome of Group 3 tumors, our data show a strong association between active enhancers and the presence of both OTX2 and the transcription factor NEUROD1. Downregulation of *OTX2* or *NEUROD1* results in reductions in markers of enhancer activity at these sites, demonstrating a significant contribution to chromatin states. Moreover, OTX2 is capable of operating as a pioneer factor at these active sites because introduction of OTX2 into primary mesenchymal stem cells (MSC) results in *de novo* induction of enhancers. Finally, among highly responsive OTX2 target genes, we identified the NEK2 kinase and found that Group 3 medulloblastoma cell lines are highly sensitive to either *NEK2* knockdown or inhibition of its kinase activity. Thus, our studies show that OTX2 is a major activator of regulatory elements in Group 3 medulloblastoma and controls genes involved in cell growth and survival.

RESULTS

A Large Set of Enhancers Is Consistently Active in Primary Group 3 Medulloblastomas

In order to define the regulatory landscape of Group 3 medulloblastoma, we mapped the genome-wide binding profiles of four histone modification marks from five fresh-frozen primary tumors and two cell lines using chromatin immunoprecipitation followed by deep sequencing (ChIP-seq) and combined these epigenomic profiles with RNA expression levels measured by RNA sequencing (RNA-seq) in the same samples. The histone modifications profiled were histone H3 lysine 4 trimethylation (H3K4me3, associated with active promoters); H3 lysine 4 monomethylation (H3K4me1, associated with enhancers); H3 lysine 27 trimethylation (H3K27me3, associated with Polycomb repression); and H3 lysine 27 acetylation (H3K27ac, associated with increased enhancer activity).

We first classified promoters into four groups based on active (H3K4me3) and repressive (H3K27me3) histone marks: active sites with H3K4me3 only, repressed sites with H3K27me3 only, and sites that are either positive or negative for both marks (Supplementary Fig. S1A and S1B). As expected, gene expression in tumor tissues was associated with promoter chromatin states (Supplementary Fig. S1C).

Given the key role of enhancer elements in orchestrating transcriptional programs, we next identified a set of 9,621 consistently active distal regulatory elements based on the presence of the H3K27ac activation mark (MACS q value 0.01) in four of five tumor samples and the absence of the H3K4me3 promoter mark (Fig. 1A, Supplementary Fig. S1D–S1F and Supplementary Table S1). The majority of these sites were found either in introns (53%) or in intergenic regions (41%; Supplementary Fig. S1G). Similar H3K27ac signals were also detected in more than 80% of these active enhancers in two Group 3 medulloblastoma cell lines (D341 and D283; Fig. 1A and Supplementary Fig. S1H and S1I) in accordance with their previous classification based on expression profiling (28). Targets of active enhancers include genes known to be specifically expressed in Group 3 medulloblastoma such as *NEUROG1* and *TULP1*, shown in Fig. 1B. Overall, the set of consistently active Group 3 enhancers was associated with higher average expression levels for their nearest genes compared with other transcripts (Fig. 1C), indicating that these regulatory elements have significant effects on transcription in primary tumors and cell lines.

OTX2 Is Present at Most Active Enhancers in Group 3 Medulloblastoma

To identify factors that control enhancer activity in Group 3 tumors, we performed motif enrichment analysis of the underlying DNA sequences. The motif recognized by the transcription factor OTX2 was the most significantly enriched in our set of 9,621 consistently active Group 3 medulloblastoma enhancers (Fig. 1D). This was also the case in all active enhancers of each of the five primary tumors considered individually (Supplementary Fig. S2). Similar results were obtained for the two Group 3 cell lines D283 and D341 (Supplementary Fig. S2). In accordance with these findings, genome-wide chromatin accessibility detected by Assay

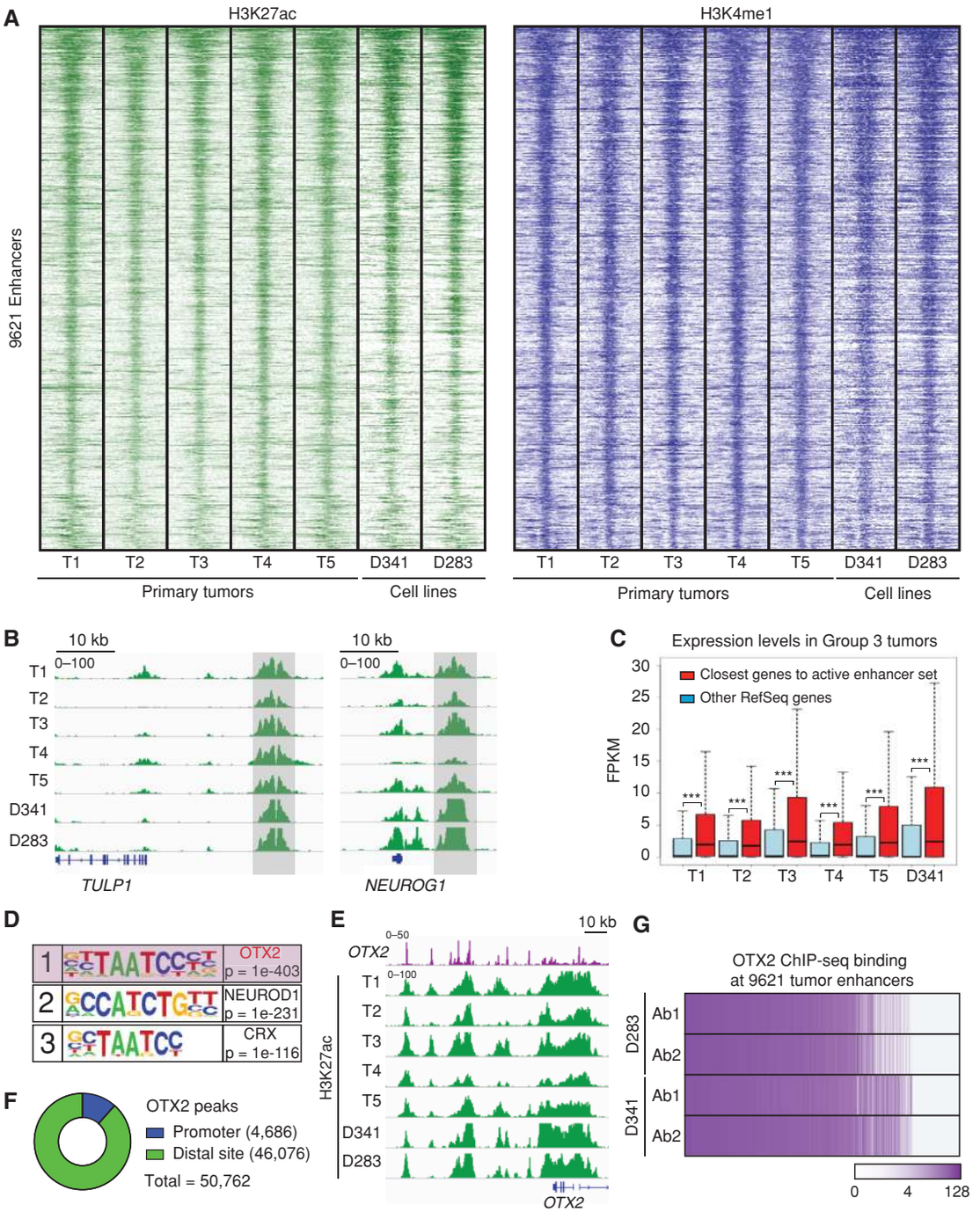

Figure 1. The majority of active enhancers shared by primary Group 3 medulloblastomas are bound by the transcription factor OTX2. **A,** Identification of a set of 9,621 shared active enhancers in primary Group 3 medulloblastoma tumors. Heatmaps depict H3K27ac (green) and H3K4me1 (blue) ChIP-seq signals in five frozen primary medulloblastoma tumors. Similar chromatin signals are found in two Group 3 cell lines (D341 and D283). Each row shows a 10-kb region centered on the active enhancer coordinates, ranked by average H3K27ac signals. **B,** Two examples of the set of active enhancers shared by Group 3 medulloblastoma tumors. H3K27ac ChIP-seq signals are shown in green, and consistently active regions are marked in light gray. **C,** Genes associated with the Group 3 active enhancer set are expressed at higher levels in primary tumors and in the D341 cell line. Boxplot of RNA-seq FPKM expression values for genes closest to Group 3 active enhancers (red) compared with other loci (blue). ***, $p < 1e{-}20$. **D,** Motif analysis of the active Group 3 enhancer set. OTX2 has the highest enrichment. **E,** The *OTX2* locus is highly active in primary tumors and cell lines and also contains several OTX2 peaks. H3K27ac ChIP-seq signals are shown in green. OTX2 ChIP-seq in D341 is shown in purple. **F,** OTX2 is primarily localized at putative enhancer sites in Group 3 medulloblastoma cell lines. Pie chart showing OTX2 peaks annotated using the RefSeq promoter database and H3K4me3 ChIP-seq data. **G,** OTX2 is present at the majority of Group 3 active enhancers defined in primary tumors. The chart represents OTX2 ChIP-seq signals overlapping the genomic coordinates of the active Group 3 enhancer set. The color scale represents $\log_2$ ChIP-seq signals. Endogenous OTX2 was profiled in two Group 3 cell lines using two different antibodies.

for Transposase-Accessible Chromatin using sequencing (ATAC-seq) in the D283 cell line also showed OTX2 as the top motif for open chromatin locations (Supplementary Fig. S3A–S3D). The motifs recognized by the transcription factors CRX, NEUROD1, and NF1 were also enriched in these analyses, albeit at considerably lower levels of significance when compared with OTX2 (Supplementary Figs. S2 and S3C). Thus, several methodologies show that OTX2 is a major feature of the Group 3 regulatory landscape.

OTX2 is a homeobox transcription factor essential for normal brain development that is induced during embryonic stem cell differentiation, and plays a crucial function in enhancer activation in this setting (29–31). In medulloblastoma, *OTX2* has been shown to be expressed in all non-SHH subtypes, and the highest levels are observed in Group 3 tumors (25). In addition, amplifications have been demonstrated in some Group 3 cases (5, 24, 27, 32). More recently, the presence of a super-enhancer has also been reported in the *OTX2* locus in medulloblastoma (23). Accordingly, we found that the *OTX2* genomic region is covered by a large group of active enhancers in our tumor samples, as well as in the two cell lines D283 and D341 (Fig. 1E). Several studies have shown that *OTX2* plays an important role in cell proliferation and survival of medulloblastoma cells (24, 25), but the direct mechanisms responsible for these properties are not well defined.

To assess the role of OTX2 in shaping the Group 3 medulloblastoma epigenetic landscape, we first mapped endogenous OTX2 genome-wide binding sites by ChIP-seq. A total of 50,762 highly reproducible OTX2 peaks were present in two Group 3 cell lines (D283 and D341) using two different antibodies (Supplementary Fig. S4A and Supplementary Table S2). This is consistent with prior studies showing large numbers of binding sites for this transcription factor (33). The majority of OTX2 binding sites were found at putative enhancer regions (91%), whereas only a small fraction were present at promoters (9%; Fig. 1F and Supplementary Fig. S4B–S4D). We next compared our set of consistently active Group 3 tumor enhancers with endogenous OTX2 binding sites and found a remarkable degree of overlap. Our data show that a full 62% of active Group 3 enhancers contain OTX2 peaks in all our conditions (Fig. 1G). Thus, as suggested by our *in silico* motif analysis, direct profiling of OTX2 binding sites shows that OTX2 is present at the majority of consistently active enhancers in Group 3 medulloblastoma.

Given that *OTX2* is most highly expressed in Group 3 tumors but is also expressed in WNT and Group 4 tumors, we considered whether the latter subtypes share part of the active enhancer landscape observed in Group 3 tumors. Analysis of an independent dataset of medulloblastoma chromatin profiles (23) was highly consistent with our results and showed strong average H3K27ac signals in Group 3 tumors at OTX2 sites overlapping our set of active enhancers (85%; Supplementary Fig. S4E). A significant but smaller fraction of these sites were also active in WNT and Group 4 tumors (61% and 62%, respectively). In contrast, only a minority of sites (30%) showed high H3K27ac levels in SHH tumors, which have low *OTX2* levels (Supplementary Fig. S4E). Thus, *OTX2* expression is associated with similarities in the enhancer landscape of non-SHH medulloblastoma tumors, suggesting that this transcription factor has a significant impact on regulatory activity in these medulloblastoma subtypes. Our comparison of H3K27ac signals also identified OTX2 sites that are specifically active in Group 3 tumors (Supplementary Fig. S4F). The majority of genes associated with these sites (69%) were expressed at higher levels in Group 3 tumors when compared with other medulloblastoma subtypes in an independent microarray expression dataset (ref. 10; Supplementary Fig. S4G), suggesting that differential OTX2 activity is linked to differences in gene expression among medulloblastoma subtypes.

Active OTX2-Bound Enhancers Are Enriched for the Transcription Factor NEUROD1 and Are Often Arranged in Clusters

Despite its strong association with active enhancers, a large number of OTX2 binding sites were outside of the set of active Group 3 enhancers and contained low levels of the H3K27ac activation mark (Supplementary Figs. S4D and S5A). In order to test for differences between OTX2 peaks with either high or low H3K27ac, we defined two contrasting categories of OTX2-bound sites (Active and Inactive) based on consistently high H3K27ac (top third of the signal distribution in 4 of 5 tumors and both cell lines, 7,053 Active peaks) or the absence of significant H3K27ac signals (bottom third in 4 of 5 tumors and both cell lines, 5,751 Inactive peaks, Fig. 2A). One example of each category is shown in Fig. 2B. Although H3K27ac levels varied over a 30-fold range between these two categories, OTX2 signals were only modestly lower on Inactive sites (Supplementary Fig. S5B). H3K4me1 and open chromatin signals (measured by ATAC-seq) were lower but readily detectable in the Inactive set (Supplementary Fig. S5B–S5D), suggesting that OTX2 is generally associated with basal enhancer features. In contrast, RNA-seq data for cell lines and primary tumors showed strong differences in expression of neighboring genes between these two categories of OTX2 binding sites, pointing to a significant functional impact on gene regulation (Fig. 2C). Thus, our data show widespread binding of OTX2 on the genome that is linked to strikingly different effects on chromatin and gene regulation.

We then searched for factors that may contribute to different H3K27ac levels at OTX2 binding sites. Upon scanning the underlying sequences of Active and Inactive OTX2 peaks, we found similar frequencies of OTX2 motif occurrences (>95% of peaks in each category contained at least one motif occurrence). In contrast, motif enrichment analysis comparing Active and Inactive OTX2 binding sites showed a strong enrichment for co-occurrence of the binding motif for NEUROD1, a bHLH transcription factor implicated in neural development (Fig. 2D, top, and Supplementary Fig. S5E), and which has been shown to be expressed in medulloblastoma (34). This cooperation was confirmed by direct profiling of endogenous NEUROD1 by ChIP-seq (Fig. 2D, bottom) and reciprocal coimmunoprecipitation experiments for the endogenous proteins (Fig. 2E). Indeed, NEUROD1 signals measured at OTX2 peaks were strongly associated with the levels of H3K27ac, suggesting that these transcription factors cooperate to activate enhancers in medulloblastoma (Fig. 2F).

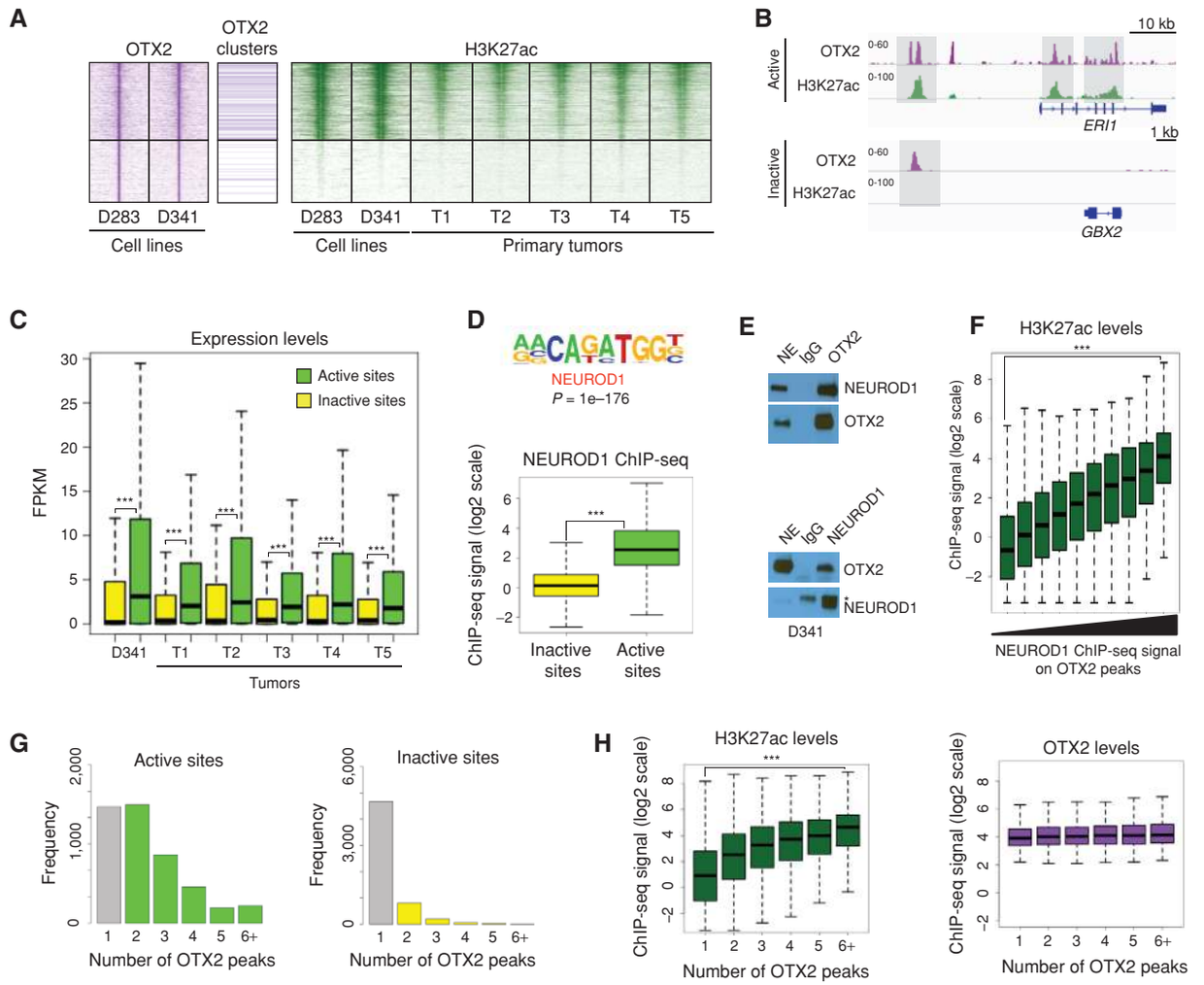

Figure 2. OTX2 is associated with higher levels of activity when paired with NEUROD1 and arranged in clusters. **A,** OTX2-bound distal sites show a wide range of H3K27ac levels. Heat maps depicting OTX2 ChIP-seq (purple) in cell lines and H3K27ac ChIP-seq (green) in cell lines and tumors. Sites where OTX2 is arranged as clusters of at least three peaks are marked. Rows are ordered by the average H3K27ac levels in cell lines and tumors and show a 10-kb region centered on each OTX2 binding site. Two categories of sites are shown: consistently Active sites (top; $n = 7{,}053$) and consistently Inactive sites (bottom; $n = 5{,}751$). **B,** One example of each category of OTX2 binding sites in D341 cell line: Active site (top) and Inactive site (bottom). OTX2 ChIP-seq signals are shown in purple, and H3K27ac ChIP-seq signals are shown in green. **C,** *OTX2* enhancer activity is linked to higher gene expression levels in medulloblastoma primary tumors and D341 medulloblastoma cells. FPKM levels of the closest genes in each category of OTX2 peak: Active (green) and Inactive (yellow). ***, $p < 1e{-}20$. **D,** NEUROD1 is enriched at active OTX2 sites. Top, motif analysis comparing Active vs. Inactive OTX2 binding sites shows that the NEUROD1 motif is the most highly enriched in Active sites. Bottom, box plot of endogenous NEUROD1 ChIP-seq signal intensities shows higher levels of NEUROD1 on Active (green) OTX2 sites compared with Inactive sites (yellow) in D341 cells. ***, $p < 1e{-}20$. **E,** OTX2 and NEUROD1 are part of the same endogenous protein complexes in medulloblastoma cells. Coimmunoprecipitation experiments in D341 nuclear extracts (NE) show an interaction between OTX2 and NEUROD1. NEUROD1 signals are detected after OTX2 immunoprecipitation (top), and reciprocal experiments show OTX2 signals after NEUROD1 immunoprecipitation (bottom). * indicates signals for IgG heavy chains used for immunoprecipitation. **F,** NEUROD1 signals on OTX2 binding sites are associated with higher levels of enhancer activity. Box plot showing H3K27ac ChIP-seq signal levels on OTX2 peaks categorized by NEUROD1 ChIP-seq signal levels in D341 cells. ***, $p < 1e{-}20$. **G,** OTX2 binds as clusters of peaks on Active enhancers. Histograms show the number of OTX2 peaks identified in a 5-kb window around each OTX2 peak in Active (left) and Inactive distal sites (right). **H,** OTX2 peak clusters have higher levels of enhancer activity. Box plots show H3K27ac (green) and OTX2 (purple) ChIP-seq levels on OTX2 binding sites according to the number of neighboring OTX2 peaks. ***, $p < 1e{-}20$.

Similarly, H3K27ac ChIP-seq signals were significantly higher at sites with both NEUROD1 and OTX2 compared with NEUROD1 alone (Supplementary Fig. S5F).

Finally, we also noticed that OTX2 was often organized as clusters of three or more peaks on Active enhancers, whereas it was mostly found as isolated peaks on Inactive distal sites (Fig. 2A and G; 37% of Active sites have OTX2 clusters vs. 5% of Inactive sites). Indeed, H3K27 acetylation increased with the number of OTX2-bound sites within 5 kb of each other (Fig. 2H), suggesting that the genomic organization of OTX2 binding sites may also contribute to activation levels of bound enhancers.

Together, our results show that, although OTX2 has a widespread presence in the genome of Group 3 medulloblastomas, only a fraction of OTX2 binding sites are associated with enhancer and neighboring gene activity. Strong marks of enhancer activity, measured by H3K27ac levels, are consistently present in a subset of OTX2 binding sites, which are distinguished by the coordinated presence of NEUROD1 and a clustered arrangement of OTX2 signals.

Both OTX2 and NEUROD1 Contribute to Enhancer Activation Levels

The wide range of H3K27ac levels associated with OTX2 binding sites prompted us to assess the direct contribution of OTX2 to this chromatin mark. In accordance with previous studies, shRNA or CRISPR/Cas9-mediated depletion of *OTX2* results in striking decreases in cell growth and viability of medulloblastoma cells (Supplementary Fig. S6A and S6B). We thus focused our analysis on the earliest time point after infection and selection (5 days), to highlight the most responsive OTX2 binding sites and their associated target genes.

The results of two independent shRNA knockdown experiments were highly consistent and showed that decreased *OTX2* levels were associated with strong reductions in H3K27ac in D341 cells (Fig. 3A, correlation coefficient 0.76). Although OTX2 has been previously associated with transcriptional repression in some systems (26, 35, 36), we did not observe significant increases in H3K27ac at direct binding sites to suggest a direct repressive effect on this chromatin mark (Fig. 3A). Active OTX2 sites showed marked decreases in H3K27ac upon *OTX2* loss, whereas sites initially devoid of H3K27ac remained mostly unaffected in D341 and D283 cells (Fig. 3B and C; Supplementary Fig. S6C and S6D). Similar chromatin results were obtained after CRISPR/Cas9-mediated *OTX2* knockout in D341 cells (Supplementary Fig. S6E–S6H, correlation coefficient 0.69). OTX2 thus operates primarily as an activator of regulatory elements and makes major contributions to H3K27ac levels at its binding sites.

Given our finding that Active OTX2 binding sites are enriched for NEUROD1, we also tested whether NEUROD1 can contribute to H3K27ac levels at these locations. As in the case of *OTX2*, knockdown of *NEUROD1* strongly decreased the viability of medulloblastoma cells, suggesting that NEUROD1-mediated gene regulation is critical for tumor survival (Supplementary Fig. S6I). Similarly to *OTX2*, we focused our analysis on early timepoints after *NEUROD1* knockdown and noted marked decreases of H3K27ac levels at many

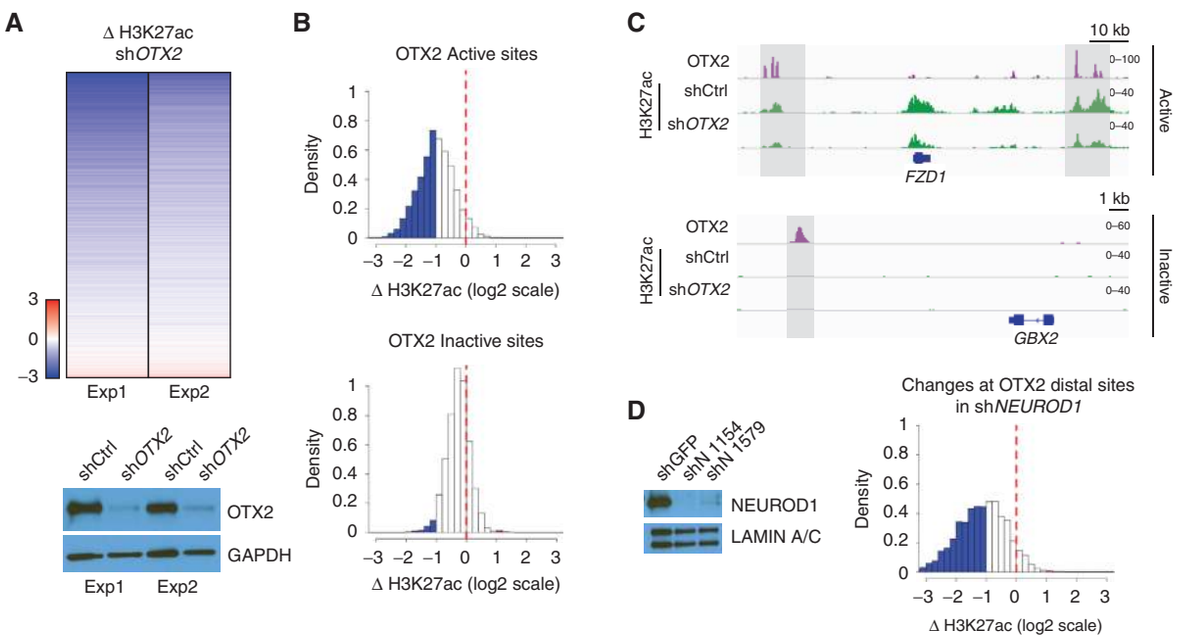

Figure 3. OTX2 maintains enhancer activity in Group 3 medulloblastoma and can operate as a pioneer factor in primary cells. **A,** OTX2 is required to maintain marks of enhancer activity in D341 medulloblastoma cells. Top, a heat map shows changes in H3K27ac ChIP-seq at distal sites with decreased OTX2 binding following knockdown with lentiviral shRNA (19,513 sites are shown). Bottom, immunoblotting for OTX2 in the two D341 knockdown experiments shows decreases in OTX2 protein levels. **B,** Depletion of OTX2 has a strong effect on chromatin states of Active OTX2 sites compared with Inactive sites. Histograms show changes in H3K27ac at sites with decreased OTX2 after infection of D341 medulloblastoma cells with shRNA lentiviruses. Top, H3K27ac decreases in Active sites after OTX2 depletion ($n = 2,649$). Bottom, Inactive sites are mostly unaffected by OTX2 depletion ($n = 2,240$). The red line indicates no variation; blue bars correspond to more than 2-fold decrease and red bars to more than 2-fold increase. **C,** Examples of ChIP-seq tracks of H3K27ac on Active and Inactive OTX2 distal sites following OTX2 knockdown in D341 medulloblastoma cells. OTX2 is shown in purple and H3K27ac in green. Regions of interest are shown in light gray. **D,** Depletion of NEUROD1 affects chromatin states at OTX2-bound enhancers. Left, NEUROD1 immunoblotting in D341 knockdown experiments. Right, histogram plot showing H3K27ac ChIP-seq changes at OTX2 distal sites with decreased NEUROD1 after infection of D341 medulloblastoma cells with lentiviral shRNA (3,377 sites are shown). The red line indicates no variation; blue bars correspond to more than 2-fold decrease and red bars to more than 2-fold increase. (*continued on next page*)

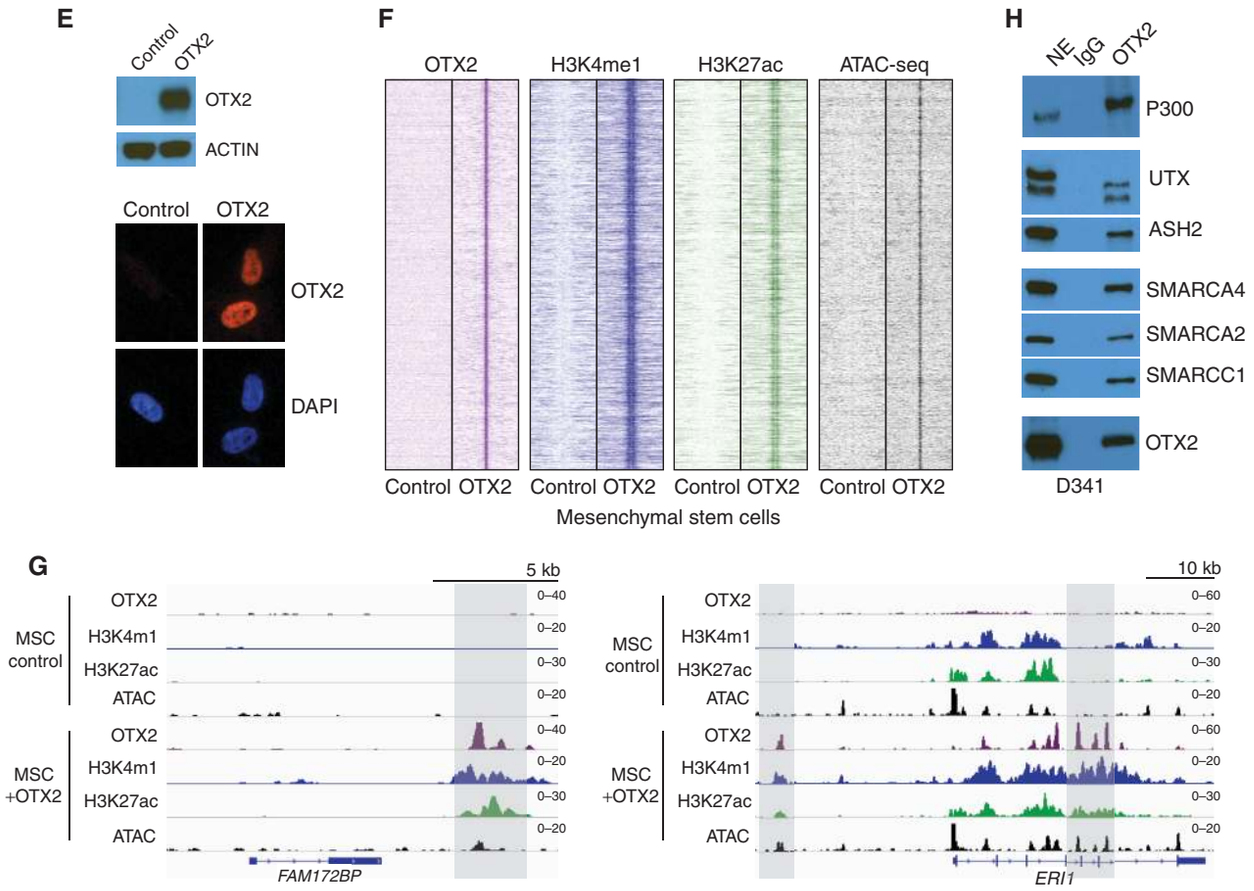

Figure 3. ***(Continued)*** **E,** Expression of ectopic OTX2 in primary MSCs. Top, OTX2 protein is detected in MSCs after lentiviral infection. Bottom, immunofluorescence demonstrates the absence of OTX2 signals in control cells and the presence of nuclear signals after introduction of ectopic OTX2 in MSCs (72 hours after infection). **F,** OTX2 creates medulloblastoma enhancers *de novo* in MSCs. Heat maps depict OTX2 (purple), H3K4me1 (blue), and H3K27ac (green) ChIP-seq signals as well as ATAC-seq (black) on 12,286 *de novo* enhancers 72 hours after OTX2 expression in MSCs. Each row shows a 10-kb region centered on OTX2 binding sites in medulloblastoma. **G,** Examples of OTX2 induced *de novo* enhancer creation in MSCs. OTX2 (purple), H3K4me1 (blue), and H3K27ac (green) ChIP-seq as well as ATAC-seq (black). Regions of interest are shown in light gray. **H,** OTX2 interacts with chromatin-modifying complexes associated with enhancer chromatin states. Coimmunoprecipitation experiments were performed in D341 nuclear extracts and show interactions with components involved in chromatin opening (SMARCA4, SMARCA2, and SMARCC1), and deposition of the enhancer marks H3K4me1 (UTX, ASH2) and H3K27ac (p300).

OTX2-bound distal sites (Fig. 3D and Supplementary Fig. S6J and S6K). Thus, NEUROD1 makes significant contributions to H3K27ac levels at a subset of OTX2 sites, consistent with cooperation between these transcription factors in the activation of enhancers. Taken together, data from our knockdown experiments show that OTX2 makes major contributions to enhancer activation and cooperates with NEUROD1 to maintain enhancer function.

OTX2 Can Operate as a Pioneer Factor to Activate Enhancer Sites *De Novo*

To further test the direct effects of OTX2 on chromatin, we ectopically expressed this transcription factor using lentiviral vectors in MSCs, a non-neural cell type that has been shown to have a permissive chromatin environment in various reprogramming studies. In contrast to other primary stem cell models such as embryonic stem cells and neural stem cells, MSCs do not express either *OTX2* or *NEUROD1* (Fig. 3E and Supplementary Fig. S7A) and thus allowed us to test the effects of OTX2 in isolation. After expression, OTX2 binding was detected at a majority of sites (65%) identified in medulloblastoma (Supplementary Fig. S7B). To highlight OTX2-dependent events, we focused our attention on approximately 19,000 genomic sites bound by OTX2 and devoid of detectable H3K4me1 basal enhancer marks in control MSC conditions. These sites were also characterized by the absence of signals for open chromatin by ATAC-seq (Fig. 3F). Remarkably, the introduction of *OTX2* was followed by profound chromatin changes at 66% of these sites, including chromatin opening and the widespread *de novo* induction of enhancer activation marks resembling those observed in medulloblastoma (Fig. 3F and G). In keeping with these results, coimmunoprecipitation experiments showed that OTX2 can interact with members of several complexes known to be involved in chromatin remodeling and enhancer activation, including the

acetyltransferase EP300 (associated with H3K27ac deposition at enhancers), as well as members of the H3K4 methyltransferase MLL complexes (UTX and ASH2, associated with H3K4me1) and the BAF chromatin remodeling complex (SMARCA4, SMARCA2, and SMARCC1, associated with chromatin opening; Fig. 3H and Supplementary Fig. S7C). Thus, OTX2 is capable of interacting with a variety of chromatin remodeling complexes that may account for its ability to activate medulloblastoma enhancers *de novo*.

Using a similar approach, we also tested the contribution of each transcription factor at enhancer sites co-occupied by NEUROD1 and OTX2 in medulloblastoma. Our results show that OTX2 was able to bind 59% of these sites, whereas NEUROD1 could bind only 20% after introduction into MSCs (Supplementary Fig. S7D), indicating a difference in the ability of these transcription factors to access these locations. Among sites devoid of detectable H3K4me1 basal enhancer marks in control conditions, OTX2 could activate almost 4-fold more sites than NEUROD1 (n = 1,788 vs. n = 479), and a subset could be activated by either OTX2 or NEUROD1 (n = 477; Supplementary Fig. S7E). These results show that NEUROD1 can make contributions to enhancer activity by itself but is significantly less powerful than OTX2 at inducing chromatin remodeling at enhancers defined in medulloblastoma.

The Mitotic Kinase NEK2 Is a Critical OTX2 Target Gene and Is Associated with Cell Survival in Medulloblastoma

Because it is well established that OTX2 regulates cell growth in medulloblastoma cells, we next sought to identify specific target genes that may contribute to this property by analyzing coordinated changes in chromatin and gene expression. To achieve this, we performed RNA-seq following acute *OTX2* knockdown in D341 medulloblastoma cells and integrated H3K27ac changes at OTX2 binding sites with gene expression changes at their nearest genes. As expected, changes in H3K27ac at the set of Active OTX2 distal sites were associated with decreases in expression levels of neighboring genes (Fig. 4A).

We next selected loci with significant changes in chromatin and significant decreases in gene expression (Fig. 4B and Supplementary Table S3). Gene Set Enrichment Analyses showed enrichment in genes involved in controlling cell growth such as *POLA2*, *RPA3*, *WEE1*, and *ECT2* (Supplementary Fig. S8A). We further refined this list by focusing on the set of genes that was highly expressed in Group 3 tumors compared with normal cerebellum in a previously published microarray dataset (ref. 4; Supplementary Fig. S8B and Supplementary Table S4). Among these genes, we identified *WEE1* and *NEK2* (Supplementary Fig. S8B and S8C), two kinases that represent potential therapeutic targets. WEE1 inhibitors have been recently shown to significantly reduce the survival of medulloblastoma cells (37), supporting the notion that OTX2 target genes may play important roles in cell survival in this disease.

To further support this concept, we set out to test the role of *NEK2* in the survival of medulloblastoma cells. NEK2, which has been implicated in the regulation of centrosome separation and microtubule organization (38), is highly expressed in various cancers but has not been studied in medulloblastoma. The *NEK2* locus is associated with several OTX2-bound active enhancers (Fig. 4C), which showed a rapid decrease in H3K27 acetylation levels after knockdown (Supplementary Fig. S8D). *NEK2* downregulation observed in RNA-seq experiments was confirmed by RT-qPCR in both D341 and D283 cell lines upon *OTX2* knockdown (Fig. 4D) and in D341 upon *OTX2* knockout (Supplementary Fig. S8E), showing that the expression of this gene is highly responsive to OTX2 levels. We then tested the effects of *NEK2* depletion using three different shRNAs and observed strong decreases in medulloblastoma cell viability upon knockdown (Fig. 4E and Supplementary Fig. S8F). In contrast, only a minority of 216 cancer cell lines in a recent shRNA screen (39) were sensitive to depletion of *NEK2* in experiments that included one of the shRNAs used in our studies (Supplementary Fig. S8G). Finally, as a proof of concept, we tested the sensitivity of medulloblastoma cell lines to the recently described small-molecule NEK2 inhibitor JH295 (40) and found that D341 and D283 cells were significantly more sensitive than unrelated control cells to NEK2 inhibition (Fig. 4F). Our experiments thus show that OTX2 target genes can have significant effects on the growth of medulloblastoma cells and may represent an attractive set of candidate therapeutic targets for the treatment of Group 3 medulloblastoma and possibly other non-SHH medulloblastoma subtypes.

DISCUSSION

Our genome-wide maps of chromatin states in Group 3 medulloblastoma show that OTX2 is a major feature of the regulatory landscape of these tumors. In keeping with OTX2 binding data from prior studies, our profiles show a large number of OTX2 binding sites across the genome (33). The combination of these profiles with our data on enhancer activation marks and knockdown studies further shows that OTX2 is found at 62% of consistently active enhancers in primary Group 3 tumors and that it makes significant contributions to enhancer activation states. Together with the fact that *OTX2* is required for the survival of medulloblastoma cells, our studies point to a critical functional role for OTX2 in the regulatory landscape of Group 3 medulloblastoma.

Although *OTX2* expression is highest in Group 3 tumors, significant levels are also observed in the WNT and Group 4 subtypes. In accordance with this expression pattern, our data show that a considerable fraction of OTX2-bound enhancers identified in Group 3 tumors are also active in WNT and Group 4 tumors and thus suggest that OTX2 may also play an important role in the regulation of gene expression programs in these other medulloblastoma subtypes. In addition to these shared sites, we also identified approximately 1,000 enhancers that are highly active specifically in Group 3 tumors, indicating that the effects of OTX2 are dependent on differences in expression levels among subtypes or other modifying factors.

Remarkably, ectopic expression in primary cells also shows that OTX2 is capable of operating as a pioneer factor to induce active enhancers resembling those observed in Group 3

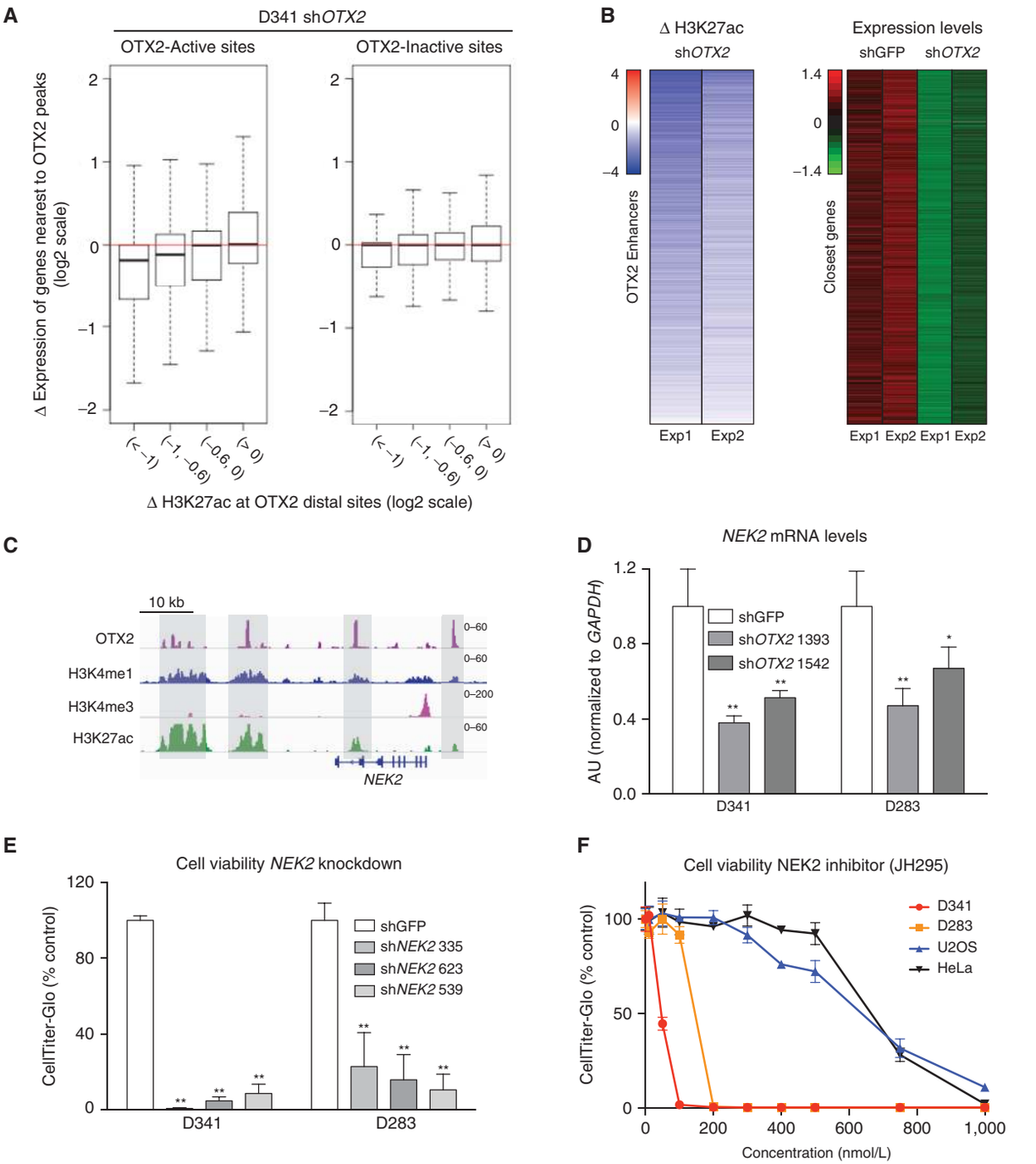

Figure 4. OTX2-dependent enhancer activity is associated with changes in the expression of target genes, including the mitotic kinase NEK2. **A,** Genes close to OTX2 distal sites are sensitive to decreased OTX2 expression. Box plot comparing changes in H3K27ac at sites with decreases in OTX2 binding after shRNA depletion with changes in the expression of closest genes in D341 cells. H3K27ac decreases are associated with reductions in expression of target genes. The effect is most evident in OTX2 Active sites ($p = 5.65e{-}12$ for Wilcoxon rank test between the first and fourth intervals). **B,** Identification of a set of highly OTX2-responsive genes through integration of epigenomic and expression profiles. Heat maps show significant chromatin changes and significant decreases in expression in genes regulated by OTX2-bound distal elements (FDR q value = 0.2). Left, H3K27ac changes at distal sites in two experiments ($n = 1{,}347$ OTX2 enhancers). Right, Z scores of gene expression levels in matching genes for two control (shGFP) and two *OTX2* shRNA depletion experiments ($n = 510$ genes). **C,** Chromatin states at the *NEK2* locus. ChIP-seq tracks showing OTX2 (purple), H3K4me1 (blue), H3K4me3 (pink), and H3K27ac (green) in D341 cells. **D,** *NEK2* expression is sensitive to OTX2 levels. RT-qPCR measuring *NEK2* mRNA levels in D341 and D283 cell lines 5 days after infection with lentiviral shRNAs targeting OTX2. **, $p < 0.01$; *, $p < 0.05$. **E,** *NEK2* knockdown affects medulloblastoma cell growth. Cell viability assays 14 days after infection in D341 and D283 cell lines with three specific shRNA targeting *NEK2*. **, $p < 0.01$. **F,** Medulloblastoma cell lines are sensitive to NEK2 inhibition. Cell viability assays 5 days after treatment with the indicated concentrations of NEK2 inhibitor JH295 in the medulloblastoma cell lines D341 and D283 and the non-medulloblastoma cell lines U2OS and HeLa.

tumors. The fact that many of these sites start with a closed chromatin conformation implies that the introduction of OTX2 can initiate a set of coordinated chromatin remodeling activities, including chromatin opening and the deposition of marks of enhancer activity. In support of this, immunoprecipitation experiments show interactions between OTX2 and components of several complexes involved in enhancer function, such as BAF, MLL, and p300. The pioneer function of OTX2 also raises the possibility that a large fraction of the regulatory landscape of medulloblastoma cells could be the result of the pathogenic overexpression of *OTX2*. Given that the cell of origin of Group 3 tumors has not been defined, the widespread presence of OTX2 in the genome could be either a reflection of high expression in a cell of origin or a pathogenic event that alters the normal expression patterns of this transcription factor. Amplification of *OTX2*, which has been observed in a fraction of Group 3 medulloblastomas, may represent such an alteration, but other mechanisms may also be involved because high *OTX2* expression levels are observed in all non-SHH tumors (5, 24, 27, 32). Importantly, our data also suggest that OTX2 may maintain its own expression by a feed-forward mechanism in tumors, because we identified multiple OTX2-bound active enhancers near the *OTX2* locus.

The high degree of heterogeneity for activation marks revealed at OTX2 binding sites by our studies further highlights the importance of coordinated chromatin profiling in testing the direct impact of transcriptional regulators. In this case, the finding that the signal intensity of OTX2 peaks is not a good predictor for the level of chromatin activation points to key contributions by additional factors. In addition, as opposed to other transcription factors that may have both activation and repressive properties, our measurement of chromatin changes after *OTX2* knockdown did not show a pattern compatible with direct repression at inactive sites. OTX2 thus appears to be a strong contributor to enhancer activation only at a subset of its binding sites.

Our data show that the presence of the transcription factor NEUROD1 and a clustered arrangement of OTX2 signals are both linked to increased activation levels at OTX2-bound distal regulatory elements. The identification of NEUROD1 as a collaborating transcription factor is of particular significance because, together with our knockdown studies showing decreased cell survival, it points to NEUROD1 as a key transcriptional mediator in Group 3 medulloblastoma. *NEUROD1* expression in medulloblastoma has been documented (34), but its function in this context was unknown. Like *OTX2*, *NEUROD1* is expressed in cerebellar precursors and affects the development of this organ (41–43), but a cooperative relationship between these transcription factors has not been established. Both transcription factors have been shown to induce and activate enhancers in separate studies in embryonic stem cells (30, 31, 44) and, in the case of OTX2, a collaborative relationship with OCT4 in these cells was proposed based on increased H3K27ac signals (30, 31). This is analogous to our finding of cooperation with NEUROD1 and suggests that OTX2 function may be modulated by specific interactions in different settings. Given that our immunoprecipitation experiments show that endogenous OTX2 and NEUROD1 are present in the same complexes in medulloblastoma, screening for agents that alter this interaction may provide a new direction for the development of future therapies.

Taken together, our studies demonstrate that the direct characterization of regulatory networks in cancer has great potential to reveal critical aspects of oncogenic programs. By focusing on consistent activation patterns at distal enhancers, our results show that the activity of OTX2 and its interaction with NEUROD1 are key regulatory events in Group 3 medulloblastoma and possibly in all non-SHH tumors. Given the importance of these transcription factors, we also expect that their direct targets would be enriched for genes with critical functions. Accordingly, cell growth pathways were enriched among the most responsive OTX2 target genes, and testing of the mitotic kinase NEK2 as a top candidate showed a strong dependency of medulloblastoma cells on the activity of this enzyme. Although more extensive testing will be necessary to validate the use of NEK2 inhibitors in medulloblastoma, our analysis of this kinase further supports the concept that genome-wide characterization of chromatin states in cancer can uncover cellular dependencies on transcription factors and their target genes that may be exploited for the development of future cancer therapies.

METHODS

Primary Tumors and Primary MSCs

Primary medulloblastoma specimens and primary MSCs were collected with approval from the Institutional Review Boards of Massachusetts General Hospital, Children's Hospital Boston, and Centre Hospitalier Universitaire Vaudois (CHUV; University of Lausanne). Samples were deidentified prior to our analysis. Group 3 subgroup classification was validated through gene expression.

Cell Culture Conditions and Drugs

Cell lines were obtained directly from the ATCC and not further authenticated. Media were obtained from Life Technologies. Human MSCs were cultured in Iscove's Modified Dulbecco's Medium containing 10% FCS and 10 ng/mL platelet-derived growth factor BB (PeproTech), as described previously (45). The medulloblastoma cell lines D341 and D283 were grown in suspension in Ultra-Low attachment cell culture flasks (Corning) in Improved Minimum Essential Medium and Eagle's Minimum Essential Medium, respectively. HeLa and U2OS were grown in DMEM. All media were supplemented with 10% FCS, and cells were cultivated at 37°C with 5% CO_2. Cells were maintained and split every 3 to 4 days according to ATCC recommendations. The NEK2 inhibitor JH295 was purchased from Millipore and reconstituted in DMSO, and single-use aliquots were conserved at −20°C.

Lentiviral Generation

Lentiviruses were produced in 293T LentiX cells (Clontech) by cotransfecting the vector of interest with the packaging vectors GAG/POL and VSVg using LT1 reagent (Mirus Bio) according to the manufacturer's instructions. Viral supernatants were collected 72 hours after transfection and concentrated using LentiX concentrator (Clontech). Virus-containing pellets were resuspended in PBS and added dropwise on cells in the presence of media supplemented with 6 μg/mL polybrene. Selection of lentivirally infected cells was achieved with puromycin

used at 0.75 to 2 μg/mL (hpMSC and medulloblastoma cell lines, respectively). Overexpression or knockdown efficiency was determined by Western blot analysis and RT-qPCR.

Quantitative RT-PCR and Western Blot Analysis

Total RNA was isolated from cells using NucleoSpin RNA (Clontech). cDNA was obtained starting from 500 ng of template and using a high-capacity RNA-to-cDNA kit (Applied Biosystems) and random hexamers. Real-time PCR amplification was performed using fast SYBR Green Master Mix (Life Technologies) and specific PCR primers in a Lightcycler 480 instrument (Roche). Oligonucleotides used are provided in Supplementary Table S5. Relative quantification of each target, normalized to an endogenous control (*GAPDH*), was performed using the comparative C_t method (Applied Biosystems). Error bars indicate SD of three technical replicates and represent at least two independent biological experiments. Statistical analyses were performed by the Student *t* test. Western blotting was performed using standard protocols. Primary antibodies used for Western blotting are listed in Supplementary Table S5. Secondary antibodies were goat anti-rabbit and goat anti-mouse immunoglobulin G-horseradish peroxidase–conjugated (Bio-Rad; 1:10,000 dilution). Membranes were developed using Western Lightning Plus-ECL enhanced chemiluminescence substrate (PerkinElmer) and visualized using photographic film.

ChIP-seq

ChIP assays were carried out on D341, D283, and MSC cultures of approximately 2 to 5 million cells per sample and per epitope, following the procedures described previously (46, 47). In brief, chromatin from formaldehyde-fixed cells was fragmented to a size range of 200 to 700 bases with a Branson 250 sonifier. Solubilized chromatin was immunoprecipitated with antibodies overnight at 4°C. Antibody–chromatin complexes were pulled down with protein G-Dynabeads (Life Technologies), washed, and then eluted. After cross-link reversal, RNase A, and proteinase K treatment, immunoprecipitated DNA was extracted with AMP Pure beads (Beckman Coulter). ChIP DNA was quantified with Qubit. ChIP DNA samples (2 to 5 ng) were used to prepare sequencing libraries, and ChIP DNA and input controls were sequenced with the Nextseq 500 Illumina genome analyzer. For primary tissue preparations, 10 to 30 mg of tumor was first cut on dry ice and chopped on ice with a razor blade. Samples were then resuspended in 1 mL cold PBS and fixed 15 minutes at room temperature by adding formaldehyde to a final concentration of 1%. Glycine was added for 5 minutes at room temperature. Samples were first washed in 1 mL cold PBS and resuspended in 1 mL cold PBS before manual homogenization with a syringe and processing as described above.

Processing of ChIP-seq Data

ChIP-seq reads were aligned to the reference genome (hg19) using BWA (48). Aligned reads were extended to 200 bp to approximate fragment sizes, and density maps were derived by counting the number of fragments overlapping each position with Integrative Genomics Viewer (IGV) tools (49). Density maps were normalized to 10 million reads. ChIP-seq coverage was visualized with IGV (50). Peaks were identified with the MACS2 peak caller (51) using matched input controls and *q* values of 10^{-2} for H3K27ac and OTX2, and 10^{-3} for NEUROD1. Peaks in blacklisted genomic regions identified by the ENCODE consortium (22) were excluded. Peak intersections were calculated using the Genomic Ranges Bioconductor package (52). Average signals for ChIP-seq data were calculated over genomic intervals using bwtools (53). Shared Group 3 medulloblastoma enhancers were defined by the overlap of H3K27ac peaks in at least four primary tumors. Regions within 1 kb of RefSeq transcription start site (TSS) locations and peaks with strong H3K4me3 signals typical of active promoters were subtracted from these intervals. OTX2 peaks were defined by the overlap of ChIP-seq signals obtained using two antibodies in two Group 3 medulloblastoma cell lines (D341 and D283). OTX2 peaks were classified as promoters if present within 1 kb of RefSeq TSSs or if they were associated with strong H3K4me3 signals. Promoter chromatin states for primary tumors were determined using H3K4me3 and H3K27me3 signals within 1 kb of each TSS to define four categories of sites: Active (at least four tumors with H3K4me3 and no tumors with H3K27me3), Repressed (at least four tumors with H3K27me3 and no tumors with H3K4me3), Bivalent (at least four tumors with both H3K4me3 and H3K27me3 signals), or lacking all signals. Positive H3K4me3 loci were defined at a relative density of 2 based on the observed signal distribution. Loci were considered positive for H3K27me3 if signals were above 2 SDs from the mean ChIP input signal. OTX2 distal sites were classified as consistently Active or Inactive if they were in the top third (Active) or bottom third (Inactive) of the distribution of H3K27ac signals for at least three primary tumors and two cell lines. Differences in peak signals between tumor types or changes after depletion of OTX2 or NEUROD1 were compared using a *t* test and corrected for multiple hypothesis testing to obtain FDR *q* values. For knockdown and CRISPR experiments, sites with 1.5-fold decreases in OTX2 and 3-fold in NEUROD1 were considered for analysis. NEUROD1 peaks were called in two Group 3 medulloblastoma cell lines (D341 and D283). Regions cobound by OTX2 and NEUROD1 were defined by the overlap of OTX2 distal sites with NEUROD1 peaks in medulloblastoma. For experiments demonstrating *de novo* enhancer induction in MSCs, we selected OTX2- or NEUROD1-bound distal sites with H3K4me1 signals below 2 SDs from the mean ChIP input signal in control cells. To identify motif occurrences in peaks, we ran TFBSTools (ref. 54; searchSeq function with min.score threshold set to 90%) in the Bioconductor package. Motif analysis and detailed peak annotation were performed with HOMER (55). For analysis of gene expression changes linked to chromatin states, peaks were assigned to the nearest TSSs of hg19 Refseq genes (excluding miRNAs).

RNA-seq and Expression Analysis

Total RNA was isolated from cells using NucleoSpin RNA (Clontech). One μg of total RNA was treated with Ribo-Zero Gold to remove ribosomal RNA. Remaining RNA was used to construct Illumina sequencing libraries with random primers according to the manufacturer's instructions using the TruSeq Stranded RNA LT Kit. Reads were aligned with the STAR aligner to hg19, and expression values were calculated using either Cufflinks (for FPKM values) or HTseq (for counts). Differential expression for knockdown experiments was calculated using DESeq2. Microarray expression data for Supplementary Fig. S2 were obtained from GEO (GSE37418; ref. 10) and for Supplementary Fig. S8 (http://archive.broadinstitute.org/pubs/medulloblastoma/cho; ref. 4).

ATAC-seq Genome-Wide DNA Accessibility Assay

ATAC-seq analysis was performed as recently described (56). Briefly, 5×10^4 cells for each condition were first incubated in hypotonic buffer then resuspended in lysis buffer, centrifuged, and resuspended in Transposase reaction mix for an additional 30 minutes at 37°C, following the manufacturer's recommendations (Nextera DNA sample Prep Kit; Illumina). After DNA purification, adaptor sequences were added to the fragmented DNA by PCR. Purified PCR products were sequenced using the Illumina NextSeq device. Paired-end reads were aligned to hg19 using BWA (48). Read start sites were adjusted to represent the center of the transposon binding event (+4 bp in the plus strand and −5 bp in the minus strand). Signal

densities were calculated over a sliding 150 bp window at 20 bp steps and normalized to 10 million reads in each experiment.

Nuclear Extract Preparation and Coimmunoprecipitation Experiments

D341 cells were first washed in PBS and swollen on ice in Buffer A (10 mmol/L Tris-HCl, pH 8, 10 mmol/L KCL, 1.5 mmol/L MgCl2 supplemented with 1 mmol/L DTT, protease/phosphatase inhibitors, Pierce, and 1 mmol/L PMSF). Cells were then lysed on ice in Buffer A containing 0.15% NP-40. Nuclei were sedimented by centrifugation and resuspended in IPH Buffer (50 mmol/L Tris-HCl, pH 8, 150 mmol/L NaCl, 5 mmol/L EDTA, 0.5% NP-40 and 10% glycerol supplemented with protease/phosphatase inhibitors, Pierce, and 1 mmol/L PMSF) before sonication in a QSONICA 800 R instrument. Nuclear protein supernatant was then collected after centrifugation for 15 minutes at 14,000 rpm and 4°C. Proteins were quantified using a Bradford assay (Pierce).

For immunoprecipitation experiments, 500 μg of nuclear lysate was diluted in IPH buffer to a final volume of 1 mL and incubated overnight at +4°C with 2 μg of the indicated antibodies in the presence of magnetic G-Dynabeads (Life Technologies) and 100 μg/mL Ethidium Bromide (Sigma-Aldrich). Beads were washed 5 times with IPH buffer and eluted by boiling in loading Laemmli buffer.

Plasmids and Antibodies

shRNAs were cloned in the pLKO.1 lentiviral backbone. The coding sequence of *OTX2* mRNA (NM_172337) was PCR amplified from D341 cells and cloned into a pENTR-D-TOPO vector before Gateway reaction into an expression vector. Guide RNAs targeting *OTX2* were cloned into the lentiviral CRISPR/Cas9 vector (Addgene #52961) following standard procedures. Sequence information and antibody references are provided in Supplementary Table S5.

Immunofluorescence Staining

Staining was performed using standard protocols. Briefly, cells were fixed in a 1x PBS solution containing 4% paraformaldehyde for 15 minutes at room temperature (RT), washed with 1x PBS, and stored at 4°C. Cells were permeabilized 10 minutes at RT in 1x PBS containing 0.5% Triton X-100, and then blocked for 30 minutes at RT, stained with OTX2 antibody for 2 hours at RT and with Alexa-Fluor 546–conjugated secondary antibody (Life Technologies) for 1 hour at RT. Cells were washed with 1x PBS between each step of the protocol. Nuclei were stained with DAPI solution.

Cell Viability Assays

Medulloblastoma and non-medulloblastoma cell lines were seeded in triplicate and grown under log phase growth conditions in Ultra-Low attachment 24-well plate and cell culture treated 96-well plate, respectively. After the indicated incubation times, cell viability was measured in triplicate using the CellTiter-Glo luminescent assay (Promega) as described by the manufacturer. Endpoint luminescence was measured on a SpectraMax M5 plate reader (Molecular Devices). The data displayed are representative of at least two biological experiments performed in duplicate or triplicate. Statistical analyses were performed by the Student *t* test.

Accession Numbers

The data accompanying this article have been deposited into GEO under accession number GSE92585.

Disclosure of Potential Conflicts of Interest

M.N. Rivera reports receiving commercial research support from Affymetrix. No potential conflicts of interest were disclosed by the other authors.

Authors' Contributions

Conception and design: G. Boulay, S.L. Pomeroy, M.N. Rivera
Development of methodology: G. Boulay
Acquisition of data (provided animals, acquired and managed patients, provided facilities, etc.): G. Boulay, M.E. Awad, T.C. Archer, W.E. Boonseng, N.E. Rossetti, B. Naigles, S. Rengarajan, A. Volorio, J.C. Kim, S.L. Pomeroy
Analysis and interpretation of data (e.g., statistical analysis, biostatistics, computational analysis): G. Boulay, N. Riggi, S. Iyer, N.E. Rossetti, J.P. Mesirov, P. Tamayo, M.J. Aryee, M.N. Rivera
Writing, review, and/or revision of the manuscript: G. Boulay, N. Riggi, T.C. Archer, J.P. Mesirov, S.L. Pomeroy, M.N. Rivera
Administrative, technical, or material support (i.e., reporting or organizing data, constructing databases): T.C. Archer, N.E. Rossetti
Study supervision: S.L. Pomeroy, M.N. Rivera
Other (completed experiments): M.E. Awad

Acknowledgments

We would like to thank Ivan Stamenkovic, Shawn Gillespie, Leah Escalante, Mario Suva, David Ebb, Nancy Tarbell, Torunn Yock, and Howard Weinstein for valuable advice and support.

Grant Support

This study was supported by research grants from A Kids' Brain Tumor Cure Foundation, aka The PLGA Foundation (to M.N. Rivera). M.N. Rivera receives research support from the V Foundation for Cancer Research. N. Riggi is supported by the Swiss National Science Foundation Professorship grant (PP00P3-157468/1) and the MEDIC Foundation. S.L. Pomeroy and J.P. Mesirov were supported by a research grant from the NCI (R01 CA109467).

The costs of publication of this article were defrayed in part by the payment of page charges. This article must therefore be hereby marked *advertisement* in accordance with 18 U.S.C. Section 1734 solely to indicate this fact.

Received July 29, 2016; revised December 21, 2016; accepted December 22, 2016; published OnlineFirst February 17, 2017.

REFERENCES

1. Ostrom QT, Gittleman H, Fulop J, Liu M, Blanda R, Kromer C, et al. CBTRUS statistical report: Primary brain and central nervous system tumors diagnosed in the United States in 2008–2012. Neuro Oncol 2015;17(Suppl 4):iv1–iv62.
2. Thompson MC, Fuller C, Hogg TL, Dalton J, Finkelstein D, Lau CC, et al. Genomics identifies medulloblastoma subgroups that are enriched for specific genetic alterations. J Clin Oncol 2006;24:1924–31.
3. Kool M, Koster J, Bunt J, Hasselt NE, Lakeman A, van Sluis P, et al. Integrated genomics identifies five medulloblastoma subtypes with distinct genetic profiles, pathway signatures and clinicopathological features. PLoS One 2008;3:e3088.
4. Cho YJ, Tsherniak A, Tamayo P, Santagata S, Ligon A, Greulich H, et al. Integrative genomic analysis of medulloblastoma identifies a molecular subgroup that drives poor clinical outcome. J Clin Oncol 2011;29:1424–30.
5. Northcott PA, Korshunov A, Witt H, Hielscher T, Eberhart CG, Mack S, et al. Medulloblastoma comprises four distinct molecular variants. J Clin Oncol 2011;29:1408–14.
6. Taylor MD, Northcott PA, Korshunov A, Remke M, Cho YJ, Clifford SC, et al. Molecular subgroups of medulloblastoma: The current consensus. Acta Neuropathol 2012;123:465–72.
7. Kool M, Korshunov A, Remke M, Jones DT, Schlanstein M, Northcott PA, et al. Molecular subgroups of medulloblastoma: An international meta-analysis of transcriptome, genetic aberrations, and clinical data

of WNT, SHH, Group 3, and Group 4 medulloblastomas. Acta Neuropathol 2012;123:473–84.
8. Pugh TJ, Weeraratne SD, Archer TC, Pomeranz Krummel DA, Auclair D, Bochicchio J, et al. Medulloblastoma exome sequencing uncovers subtype-specific somatic mutations. Nature 2012;488:106–10.
9. Northcott PA, Shih DJ, Peacock J, Garzia L, Morrissy AS, Zichner T, et al. Subgroup-specific structural variation across 1,000 medulloblastoma genomes. Nature 2012;488:49–56.
10. Robinson G, Parker M, Kranenburg TA, Lu C, Chen X, Ding L, et al. Novel mutations target distinct subgroups of medulloblastoma. Nature 2012;488:43–8.
11. Jones DT, Jager N, Kool M, Zichner T, Hutter B, Sultan M, et al. Dissecting the genomic complexity underlying medulloblastoma. Nature 2012;488:100–5.
12. Gibson P, Tong Y, Robinson G, Thompson MC, Currle DS, Eden C, et al. Subtypes of medulloblastoma have distinct developmental origins. Nature 2010;468:1095–9.
13. Takahashi K, Yamanaka S. Induction of pluripotent stem cells from mouse embryonic and adult fibroblast cultures by defined factors. Cell 2006;126:663–76.
14. Gidekel S, Pizov G, Bergman Y, Pikarsky E. Oct-3/4 is a dose-dependent oncogenic fate determinant. Cancer Cell 2003;4:361–70.
15. Hochedlinger K, Yamada Y, Beard C, Jaenisch R. Ectopic expression of Oct-4 blocks progenitor-cell differentiation and causes dysplasia in epithelial tissues. Cell 2005;121:465–77.
16. Suva ML, Rheinbay E, Gillespie SM, Patel AP, Wakimoto H, Rabkin SD, et al. Reconstructing and reprogramming the tumor-propagating potential of glioblastoma stem-like cells. Cell 2014;157:580–94.
17. Suva ML, Riggi N, Bernstein BE. Epigenetic reprogramming in cancer. Science 2013;339:1567–70.
18. Leung D, Jung I, Rajagopal N, Schmitt A, Selvaraj S, Lee AY, et al. Integrative analysis of haplotype-resolved epigenomes across human tissues. Nature 2015;518:350–4.
19. Tsankov AM, Gu H, Akopian V, Ziller MJ, Donaghey J, Amit I, et al. Transcription factor binding dynamics during human ES cell differentiation. Nature 2015;518:344–9.
20. Roadmap Epigenomics C, Kundaje A, Meuleman W, Ernst J, Bilenky M, Yen A, et al. Integrative analysis of 111 reference human epigenomes. Nature 2015;518:317–30.
21. Andersson R, Gebhard C, Miguel-Escalada I, Hoof I, Bornholdt J, Boyd M, et al. An atlas of active enhancers across human cell types and tissues. Nature 2014;507:455–61.
22. Consortium EP. An integrated encyclopedia of DNA elements in the human genome. Nature 2012;489:57–74.
23. Lin CY, Erkek S, Tong Y, Yin L, Federation AJ, Zapatka M, et al. Active medulloblastoma enhancers reveal subgroup-specific cellular origins. Nature 2016;530:57–62.
24. Di C, Liao S, Adamson DC, Parrett TJ, Broderick DK, Shi Q, et al. Identification of OTX2 as a medulloblastoma oncogene whose product can be targeted by all-trans retinoic acid. Cancer Res 2005;65:919–24.
25. Adamson DC, Shi Q, Wortham M, Northcott PA, Di C, Duncan CG, et al. OTX2 is critical for the maintenance and progression of Shh-independent medulloblastomas. Cancer Res 2010;70:181–91.
26. Bunt J, Hasselt NE, Zwijnenburg DA, Hamdi M, Koster J, Versteeg R, et al. OTX2 directly activates cell cycle genes and inhibits differentiation in medulloblastoma cells. Int J Cancer 2012;131:E21–32.
27. Northcott PA, Jones DT, Kool M, Robinson GW, Gilbertson RJ, Cho YJ, et al. Medulloblastomics: The end of the beginning. Nat Rev Cancer 2012;12:818–34.
28. Weeraratne SD, Amani V, Teider N, Pierre-Francois J, Winter D, Kye MJ, et al. Pleiotropic effects of miR-183~96~182 converge to regulate cell survival, proliferation and migration in medulloblastoma. Acta Neuropathol 2012;123:539–52.
29. Beby F, Lamonerie T. The homeobox gene Otx2 in development and disease. Exp Eye Res 2013;111:9–16.
30. Buecker C, Srinivasan R, Wu Z, Calo E, Acampora D, Faial T, et al. Reorganization of enhancer patterns in transition from naive to primed pluripotency. Cell Stem Cell 2014;14:838–53.
31. Yang SH, Kalkan T, Morissroe C, Marks H, Stunnenberg H, Smith A, et al. Otx2 and Oct4 drive early enhancer activation during embryonic stem cell transition from naive pluripotency. Cell Rep 2014;7:1968–81.
32. Boon K, Eberhart CG, Riggins GJ. Genomic amplification of orthodenticle homologue 2 in medulloblastomas. Cancer Res 2005;65:703–7.
33. Hovestadt V, Jones DT, Picelli S, Wang W, Kool M, Northcott PA, et al. Decoding the regulatory landscape of medulloblastoma using DNA methylation sequencing. Nature 2014;510:537–41.
34. Rostomily RC, Bermingham-McDonogh O, Berger MS, Tapscott SJ, Reh TA, Olson JM. Expression of neurogenic basic helix-loop-helix genes in primitive neuroectodermal tumors. Cancer Res 1997;57:3526–31.
35. Bai RY, Staedtke V, Lidov HG, Eberhart CG, Riggins GJ. OTX2 represses myogenic and neuronal differentiation in medulloblastoma cells. Cancer Res 2012;72:5988–6001.
36. Bunt J, Hasselt NA, Zwijnenburg DA, Koster J, Versteeg R, Kool M. OTX2 sustains a bivalent-like state of OTX2-bound promoters in medulloblastoma by maintaining their H3K27me3 levels. Acta Neuropathol 2013;125:385–94.
37. Harris PS, Venkataraman S, Alimova I, Birks DK, Balakrishnan I, Cristiano B, et al. Integrated genomic analysis identifies the mitotic checkpoint kinase WEE1 as a novel therapeutic target in medulloblastoma. Mol Cancer 2014;13:72.
38. Xia J, Franqui Machin R, Gu Z, Zhan F. Role of NEK2A in human cancer and its therapeutic potentials. Biomed Res Int 2015;2015:862461.
39. Cowley GS, Weir BA, Vazquez F, Tamayo P, Scott JA, Rusin S, et al. Parallel genome-scale loss of function screens in 216 cancer cell lines for the identification of context-specific genetic dependencies. Sci Data 2014;1:140035.
40. Henise JC, Taunton J. Irreversible Nek2 kinase inhibitors with cellular activity. J Med Chem 2011;54:4133–46.
41. Frantz GD, Weimann JM, Levin ME, McConnell SK. Otx1 and Otx2 define layers and regions in developing cerebral cortex and cerebellum. J Neurosci 1994;14:5725–40.
42. Miyata T, Maeda T, Lee JE. NeuroD is required for differentiation of the granule cells in the cerebellum and hippocampus. Genes Dev 1999;13:1647–52.
43. Vernay B, Koch M, Vaccarino F, Briscoe J, Simeone A, Kageyama R, et al. Otx2 regulates subtype specification and neurogenesis in the midbrain. J Neurosci 2005;25:4856–67.
44. Pataskar A, Jung J, Smialowski P, Noack F, Calegari F, Straub T, et al. NeuroD1 reprograms chromatin and transcription factor landscapes to induce the neuronal program. EMBO J 2016;35:24–45.
45. Riggi N, Suva ML, De Vito C, Provero P, Stehle JC, Baumer K, et al. EWS-FLI-1 modulates miRNA145 and SOX2 expression to initiate mesenchymal stem cell reprogramming toward Ewing sarcoma cancer stem cells. Genes Dev 2010;24:916–32.
46. Ku M, Koche RP, Rheinbay E, Mendenhall EM, Endoh M, Mikkelsen TS, et al. Genomewide analysis of PRC1 and PRC2 occupancy identifies two classes of bivalent domains. PLoS Genet 2008;4:e1000242.
47. Mikkelsen TS, Ku M, Jaffe DB, Issac B, Lieberman E, Giannoukos G, et al. Genome-wide maps of chromatin state in pluripotent and lineage-committed cells. Nature 2007;448:553–60.
48. Li H, Durbin R. Fast and accurate short read alignment with Burrows-Wheeler transform. Bioinformatics 2009;25:1754–60.
49. Robinson JT, Thorvaldsdottir H, Winckler W, Guttman M, Lander ES, Getz G, et al. Integrative genomics viewer. Nat Biotechnol 2011;29:24–6.
50. Thorvaldsdottir H, Robinson JT, Mesirov JP. Integrative Genomics Viewer (IGV): High-performance genomics data visualization and exploration. Brief Bioinform 2013;14:178–92.
51. Zhang Y, Liu T, Meyer CA, Eeckhoute J, Johnson DS, Bernstein BE, et al. Model-based analysis of ChIP-Seq (MACS). Genome Biol 2008;9:R137.
52. Lawrence M, Huber W, Pages H, Aboyoun P, Carlson M, Gentleman R, et al. Software for computing and annotating genomic ranges. PLoS Comput Biol 2013;9:e1003118.

53. Pohl A, Beato M. bwtool: A tool for bigWig files. Bioinformatics 2014; 30:1618–9.
54. Tan G, Lenhard B. TFBSTools: An R/bioconductor package for transcription factor binding site analysis. Bioinformatics 2016;32:1555–6.
55. Heinz S, Benner C, Spann N, Bertolino E, Lin YC, Laslo P, et al. Simple combinations of lineage-determining transcription factors prime cis-regulatory elements required for macrophage and B cell identities. Mol Cell 2010;38:576–89.
56. Buenrostro JD, Giresi PG, Zaba LC, Chang HY, Greenleaf WJ. Transposition of native chromatin for fast and sensitive epigenomic profiling of open chromatin, DNA-binding proteins and nucleosome position. Nat Methods 2013;10:1213–8.